J. Fluid Mech. (2014), *vol.* 752, *pp.* 107–122. © Cambridge University Press 2014
doi:10.1017/jfm.2014.324

Time-dependent Taylor–Aris dispersion of an initial point concentration

Søren Vedel[1,†], Emil Hovad[1] and Henrik Bruus[2]

[1]Department of Micro- and Nanotechnology, Technical University of Denmark, Building 345 B, DK-2800 Kongens Lyngby, Denmark

[2]Department of Physics, Technical University of Denmark, Building 309, DK-2800 Kongens Lyngby, Denmark

(Received 18 October 2012; revised 2 June 2014; accepted 4 June 2014; first published online 2 July 2014)

Based on the method of moments, we derive a general theoretical expression for the time-dependent dispersion of an initial point concentration in steady and unsteady laminar flows through long straight channels of any constant cross-section. We retrieve and generalize previous case-specific theoretical results, and furthermore predict new phenomena. In particular, for the transient phase before the well-described steady Taylor–Aris limit is reached, we find anomalous diffusion with a dependence of the temporal scaling exponent on the initial release point, generalizing this finding in specific cases. During this transient we furthermore identify maxima in the values of the dispersion coefficient which exceed the Taylor–Aris value by amounts that depend on channel geometry, initial point release position, velocity profile and Péclet number. We show that these effects are caused by a difference in relaxation time of the first and second moments of the solute distribution and may be explained by advection-dominated dispersion powered by transverse diffusion in flows with local velocity gradients.

Key words: general fluid mechanics, mathematical foundations, particle/fluid flows

1. Introduction

We have previously developed a compact and comprehensive analytical theory for the dispersion in any unsteady flow valid for any initial distribution of solute (Vedel & Bruus 2012). Motivated by the vast majority of the literature, e.g. Taylor (1953), Aris (1956), Barton (1983), Watson (1983), Mukherjee & Mazumder (1988), Ajdari, Bontoux & Stone (2006) and Paul & Mazumder (2008), that paper focused on the important special case of initial transverse uniform distribution. Here, we consider the logical next special case of an initial point distribution. Although no less important in neither practical nor theoretical regards (e.g. Fallon, Howell & Chauhan 2009), this case has attracted considerably less attention. Presumably this failing interest is, at least in part, due to its mathematical difficulty: the first treatments of the

† Present address: Niels Bohr International Academy and Center for Models of Life, Niels Bohr Institute, University of Copenhagen, Blegdamsvej 17, DK-2100 Copenhagen, Denmark. Email address for correspondence: svedel@nbi.dk

https://doi.org/10.1017/jfm.2014.324 Published online by Cambridge University Press

problem focused on steady linear shear flow (Foister & van de Ven 1980; Rhines & Young 1983), which were followed by work neglecting the confining walls for a time-oscillating linear shear flow (Leighton 1989) and steady Poiseuille flow in a circular cross-section (Latini & Bernoff 2001), before Camassa, Lin & McLaughlin (2010) recently presented steady-flow solutions for both the parallel-plate and circular cross-sections which did include the physical boundary conditions at the wall.

The framework put forth in Vedel & Bruus (2012) is easily applied to the present problem, and allows for both general conclusions independent of the specific cross-section, physical interpretation and treatment of particular channel geometries. Hence, in the following we present the general theoretical expression for the effective diffusivity D_{eff} of a point concentration valid for any steady or unsteady flow in a straight channel of any (but constant) cross-section. We focus on steady flows and only briefly touch on unsteady flows, because the latter do not lead to qualitatively different results. We identify and explain fundamental transient phenomena in D_{eff} before the well-described Taylor–Aris limit of transversely uniform solute distribution is reached by transverse diffusion.

2. The initial point distribution and its physical relevance

We consider an initial distribution of N_o solute molecules which are confined to a single point $\boldsymbol{r}_o$ in space. The initial condition $\tilde{c}$ for the dimensionfull concentration $c(\boldsymbol{r}, t)$ is

$$\tilde{c}(x, \boldsymbol{r}_\perp) = c(\boldsymbol{r}, 0) = N_o\, \delta(\boldsymbol{r} - \boldsymbol{r}_o), \tag{2.1}$$

where $\delta(\boldsymbol{x})$ is the three-dimensional Dirac delta function. This concentration is released in a long, straight and translational-invariant channel of length $\mathscr{L}$, which is parallel to the x-axis and has a constant cross-section Ω with area $\mathscr{A}$. The transverse coordinates are denoted $\boldsymbol{r}_\perp = (y, z)$ and the full coordinates as $\boldsymbol{r} = (x, \boldsymbol{r}_\perp)$. For convenience we define the origin in the axial direction by the initial solute position, so $\boldsymbol{r}_o = (0, \boldsymbol{r}_\perp^o)$.

The initial point distribution is an idealized physical model of a droplet of solute. This has practical interest as a model of e.g. drugs injected into the blood stream (Fallon *et al.* 2009) or additives injected into flows in industrial applications. Furthermore, the point distribution is the next logical step following the transverse uniform distribution in building basic physical understanding of the dispersion phenomenon and the roles of the different basic physical processes of varying fluid speed and diffusion; finally, the Dirac delta function of (2.1) has attractive mathematical properties which makes this problem analytically tractable.

3. Mathematical expression for the effective diffusivity D_{eff}

Using Aris's method of statistical moments M_i for the solute distribution, the effective diffusivity D_{eff} of a solute is determined from the time derivative of the variance $\mu_2(t)$ about the solute centre of mass (Aris 1956, 1960; Barton 1983; Mukherjee & Mazumder 1988)

$$D_{eff}(t) = \frac{1}{2}\frac{\mathrm{d}\mu_2(t)}{\mathrm{d}t} = \frac{1}{2}\frac{\mathrm{d}M_2}{\mathrm{d}t} - M_1\frac{\mathrm{d}M_1}{\mathrm{d}t}, \tag{3.1}$$

where the full moments $M_2(t)$, $M_1(t)$ and the time derivative $\mathrm{d}M_1(t)/\mathrm{d}t$ for any initial distribution are defined in (3.18) of Vedel & Bruus (2012). Owing to the time

https://doi.org/10.1017/jfm.2014.324 Published online by Cambridge University Press

derivative, the statistic $D_{eff}(t)$ in (3.1) measures the instantaneous changes to the axial dispersion of the solute (the solute variance) and thus is the natural measure for investigating time-dependent dispersion phenomena. The spatiotemporal dependencies of M_i are treated by a diffusion-eigenmode expansion in space and a Fourier expansion in time. We present only the main expressions using non-dimensional variables and refer the reader to Vedel & Bruus (2012) for the full description of the formalism.

Using the Dirac bra-ket notation for Hilbert spaces, the time-independent orthonormal basis for the spatial expansion $\big|f(x,\boldsymbol{r}_\perp,t)\big\rangle = \sum_n A_n(x,t)\,\big|f_n(\boldsymbol{r}_\perp)\big\rangle$ of any function $f(x,\boldsymbol{r}_\perp)$ consists of the diffusion eigenmodes $\big|f_n(\boldsymbol{r}_\perp)\big\rangle$ with eigenvalues λ_n defined by

$$(\lambda_n + \nabla_\perp^2)\big|f_n(\boldsymbol{r}_\perp)\big\rangle = 0, \quad n = 0,1,2,\ldots, \tag{3.2a}$$

$$\boldsymbol{n}\cdot\nabla_\perp\big|f_n(\boldsymbol{r}_\perp)\big\rangle = 0, \quad \text{on all walls}, \tag{3.2b}$$

$$\big\langle f_n|f_m\big\rangle = \delta_{n,m}, \tag{3.2c}$$

where the inner product $\langle f|g\rangle$ for function pairs $f(x,\boldsymbol{r}_\perp,t)$ and $g(x,\boldsymbol{r}_\perp,t)$ is defined as

$$\big\langle f|g\big\rangle = \frac{1}{\mathscr{V}}\int_{-\mathscr{L}/2}^{\mathscr{L}/2}\mathrm{d}x\int_\Omega \mathrm{d}\boldsymbol{r}_\perp f^*(x,\boldsymbol{r}_\perp,t)\,g(x,\boldsymbol{r}_\perp,t), \tag{3.3}$$

with $*$ indicating complex conjugation and $\mathscr{V} = \mathscr{A}\mathscr{L}$. For functions $f_\perp(\boldsymbol{r}_\perp,t)$ and $g_\perp(\boldsymbol{r}_\perp,t)$ depending only on $\boldsymbol{r}_\perp$, we obtain $\big\langle f_\perp|g_\perp\big\rangle = (1/\mathscr{A})\int_\Omega \mathrm{d}\boldsymbol{r}_\perp f_\perp^*(\boldsymbol{r}_\perp,t)g_\perp(\boldsymbol{r}_\perp,t)$, since the x-integration trivially gives unity. The index n is enumerating the eigenmodes by ascending eigenvalue, $\lambda_n \leqslant \lambda_{n+1}$. However, in the case of symmetric cross-sections, e.g. axisymmetric or mirror symmetric as in § 5, the enumeration is better done using pair indices (n,m) in which case n is replaced by (n,m) and sums $\sum_{n=0}^{\infty}$ are replaced by $\sum_{n=0}^{\infty}\sum_{m=0}^{\infty}$. We emphasize that the use of this Hilbert-space representation of the spatial dependencies does not introduce new physics, but merely serves as a convenient notation: it allows us to express our theoretical results in a compact, general and physically transparent form that is independent of the channel cross-section, and whose structure reveals how the involved processes of advection, diffusion and external actuation interact to produce the dispersion.

The physical time $\tilde{t}$ is substituted by the dimensionless time $t = D\tilde{t}/L_o^2$, where L_o is characteristic length scale and D is the solute diffusivity. The temporal dependence is then expressed by Fourier expansions in the harmonics of the dimensionless base frequency $\omega_o = L_o^2\tilde{\omega}_o/D$, where $\tilde{\omega}_o$ is a dimensionfull base frequency of the pulsatile flow. This can also be written as $\omega_o = Wo^2Sc$, where $Wo = \sqrt{L_o^2\tilde{\omega}_o/\nu}$ is the Womersley number of the pulsatile flow in the channel, $Sc = \nu/D$ is the Schmidt number and ν the kinematic viscosity (momentum diffusivity). The velocity field $\boldsymbol{v}$ in the channel is normalized by a characteristic velocity U_o and is assumed to be axis parallel, e.g. of the form $\boldsymbol{v} = u(\boldsymbol{r}_\perp,t)\boldsymbol{e}_x$. Thus, $u(\boldsymbol{r}_\perp,t)$ is represented by

$$u(\boldsymbol{r}_\perp,t) = \sum_{\ell=-\infty}^{\infty} u_\ell(\boldsymbol{r}_\perp)\,\mathrm{e}^{\mathrm{i}\ell\omega_o t}, \quad \omega_o = Wo^2Sc = \frac{L_o^2\tilde{\omega}_o}{D}, \tag{3.4}$$

where complex notation with $\mathrm{i} = \sqrt{-1}$ is introduced for the time. By demanding that $u_{-\ell}(\boldsymbol{r}_\perp) = u_\ell^*(\boldsymbol{r}_\perp)$, we ensure that the velocity field is real.

https://doi.org/10.1017/jfm.2014.324 Published online by Cambridge University Press

Using this notation, the effective diffusivity D_{eff} of (3.1) is determined by inserting the initial point distribution of (2.1) into (3.18) of Vedel & Bruus (2012). After straightforward algebra we obtain the result

$$D_{eff}^{point} = 1 + Pé^2 \sum_{n=0}^{\infty}\sum_{m=0}^{\infty}\sum_{\ell=-\infty}^{\infty}\sum_{k=-\infty}^{\infty} f_n(\boldsymbol{r}_\perp^o)\langle u_k|f_m\rangle\, \mathrm{e}^{-(\lambda_m+\mathrm{i}k\omega_o)t} \times\left[\langle f_m|u_\ell|f_n\rangle\frac{\mathrm{e}^{(\lambda_m-\lambda_n+\mathrm{i}\ell\omega_o)t}-1}{\lambda_m-\lambda_n+\mathrm{i}\ell\omega_o} + f_m(\boldsymbol{r}_\perp^o)\langle u_\ell|f_n\rangle\frac{\mathrm{e}^{-(\lambda_n+\mathrm{i}\ell\omega_o)t}-1}{\lambda_n+\mathrm{i}\ell\omega_o}\right]. \quad (3.5)$$

For the important special case of steady flow given by $|u_\ell\rangle = \delta_{\ell,0}|u_0\rangle$, this simplifies to

$$D_{eff}^{pnt,std} = 1 + Pé^2 \sum_{n=0}^{\infty}\sum_{m=0}^{\infty} f_n(\boldsymbol{r}_\perp^o)\langle u_0|f_m\rangle\, \mathrm{e}^{-\lambda_m t} \times\left[\langle f_m|u_0|f_n\rangle\frac{\mathrm{e}^{(\lambda_m-\lambda_n)t}-1}{\lambda_m-\lambda_n} + f_m(\boldsymbol{r}_\perp^o)\langle u_0|f_n\rangle\frac{\mathrm{e}^{-\lambda_n t}-1}{\lambda_n}\right]. \quad (3.6)$$

Terms of the form $(\mathrm{e}^{0t}-1)/0$ are to be interpreted as the limiting value $\lim_{q\to 0}\left[(\mathrm{e}^{qt}-1)/q\right] = t$. To facilitate some of the subsequent discussion we also give the following form of (3.6), where the $m=0$ term and $n=0$ term have been separated out explicitly,

$$\begin{aligned} D_{eff}^{pnt,std} = 1 + Pé^2\Bigg\{ &\sum_{n=1}^{\infty}\langle u_0|f_n\rangle\left[f_n(\boldsymbol{r}_\perp^o)\left(\langle f_n|u_0|f_n\rangle - \langle u_0|1\rangle\right) t\,\mathrm{e}^{-\lambda_n t}\right. \\ &\left. + \langle f_n|u_0\rangle\frac{1-\mathrm{e}^{-\lambda_n t}}{\lambda_n} + f_n^2(\boldsymbol{r}_\perp^o)\langle u_0|f_n\rangle\frac{\mathrm{e}^{-2\lambda_n t}-\mathrm{e}^{-\lambda_n t}}{\lambda_n}\right] \\ &+ \sum_{n=1}^{\infty}\sum_{\substack{m=1\\ m\neq n}}^{\infty} f_n(\boldsymbol{r}_\perp^o)\langle u_0|f_m\rangle\left[\langle f_m|u_0|f_n\rangle\frac{\mathrm{e}^{-\lambda_n t}-\mathrm{e}^{-\lambda_m t}}{\lambda_m-\lambda_n}\right. \\ &\left.\left. + f_m(\boldsymbol{r}_\perp^o)\langle u_0|f_n\rangle\frac{\mathrm{e}^{-(\lambda_m+\lambda_n)t}-\mathrm{e}^{-\lambda_m t}}{\lambda_n}\right]\right\}. \end{aligned} \quad (3.7)$$

From this expression it is obvious that we recover the well-known result from transversely uniform initial distributions (Barton 1983) in the long-time limit $t \gg 1/\lambda_1$ where all transient exponential terms have vanished,

$$D_{eff}^{point}(\infty) = D_{eff}^{unif}(\infty) = 1 + Pé^2\sum_{n=1}^{\infty}\frac{|\langle u_0|f_n\rangle|^2}{\lambda_n}. \quad (3.8)$$

The $\boldsymbol{r}_\perp^o$ dependence has dropped out since $f_0(\boldsymbol{r}_\perp) = 1$, and as expected in this limit, the initial point concentration has spread out uniformly in the transverse direction. Only in the initial transient period $t \lesssim 1/\lambda_1$ does the initial point case deviate from the transverse uniform case, and we consequently only study this period in the rest of this paper.

The infinite sums above are formal expressions that have not been analysed for general convergence properties. However, as seen in § 6 and our previous work (Vedel & Bruus 2012) we have made direct comparisons between specific theoretical predictions derived from our formal theory and direct numerical simulations, and found good agreement in all cases.

https://doi.org/10.1017/jfm.2014.324 Published online by Cambridge University Press

4. General observations on point concentration dispersion

Many features of the behaviour of $D_{eff}^{point}(t)$ are similar to the transversely uniform case $D_{eff}^{unif}(t)$, including the scaling with Pe^2, the additivity of the response to the flow frequencies, the frequency-doubled response at $2\omega_o\ell$ to any flow frequency $\omega_o\ell$, the negative values of D_{eff}^{point} at large amplitudes of the oscillating flow components, and the long-time behaviour, $t \gg 1/\lambda_1$. Negative values of D_{eff}^{point} has previously been found for point releases in unbounded harmonically oscillating linear shear flows (Leighton 1989), but the theory above shows that this is a general feature of bounded flows as well. Here D_{eff}^{point} depends on the initial release position through $f_n(\boldsymbol{r}_\perp^o)$ in any cross-section, thereby generalizing the $\boldsymbol{r}_\perp^o$-dependence found for a few specific cross-sections (Latini & Bernoff 2001; Camassa *et al.* 2010). Furthermore, and contrary to the case of transverse uniform distributions, the centre of mass initially does not move with the channel mean speed but relaxes to it on the time scale $1/\lambda_1$.

Equations (3.5) and (3.6), valid for any channel cross-section, explicitly confirm the hypothesis put forth by Latini & Bernoff (2001) and supported by Camassa *et al.* (2010) that transient anomalous diffusion – a time-dependent D_{eff}^{point} – is a hallmark of Taylor–Aris dispersion of point concentrations; this of course going beyond the transient phase of anomalous $D_{eff}^{unif} \propto t$ exhibited by transverse uniform initial distributions before they reach the steady Taylor–Aris limit. In § 6.1, we show the existence of anomalous diffusion with power-law exponents 2 and 3 in the temporal scaling of D_{eff}^{point} both by using (3.6) and by direct numerical simulation of the governing advection–diffusion equation. We find that these two methods are in quantitative agreement.

We have not been able to provide closed analytical expressions based on (3.5) and (3.6) for this anomalous diffusion behaviour of $D_{eff}^{point}(t)$. However, the prefactors $\langle u_\ell | f_m \rangle$ and $\langle f_m | u_\ell | f_n \rangle$ are decaying sufficiently rapidly to ensure convergence. For example, for the parallel-plate system detailed in § 5, the mode index for the horizontal mode is always zero, and for the vertical mode index we find for a steady Poiseuille flow that $f_m(\boldsymbol{r}_\perp^o) \propto \cos\left[m\pi(1+z_0)/2\right]$, $\lambda_m \propto m^2$, $\langle u_0 | f_m \rangle \propto m^{-2}$, $\langle f_m | u_0 | f_m \rangle \propto m^{-2}$ and $\langle f_m | u_0 | f_n \rangle \propto (m^2+n^2)/(m^2-n^2)^2$. Applying the triangle inequality on the absolute value of the double sum, an upper bound is found by setting all time-dependent factors and terms $|f_m(\boldsymbol{r}_\perp^o)|$ equal to unity resulting in convergent sums. Note, that in this argument we do not rely neither on the cut-offs supplied by the decaying exponential factors nor on the alternating signs provided by the factors $f_m(\boldsymbol{r}_\perp^o)$, two features which further speed up convergence. For general non-integrable cross-sections, we suggest that statistical estimates for D_{eff}^{point} may be obtained applying random-matrix theory on the quantities $f_m(\boldsymbol{r}_\perp^o)$, $\langle u_\ell | f_n \rangle$, and $\langle f_m | u_\ell | f_n \rangle$, a method that has been successfully applied to problems in nuclear physics and condensed matter physics (Mehta 2004).

In the rest of the paper we apply our general theory to the special cases of the circular tube and the parallel-plate channel, since we found in our previous paper that general channel cross-section geometries only deviate by having two inherent time scales but otherwise exhibit the same dynamics (Vedel & Bruus 2012).

5. Specific eigenmodes, flow fields and overlap integrals

For a circular channel of radius a, the laminar flow field of magnitude U_o is assumed to be axisymmetric, a symmetry not possessed by the concentration field

https://doi.org/10.1017/jfm.2014.324 Published online by Cambridge University Press

due to the initial point concentration. The radial coordinate is normalized by a so $0 < r < 1$ while the azimuthal angle ϕ is between 0 and 2π. The pair index eigenmodes $\big|f_{nm}\big\rangle$, flow field Fourier components $\big|u_\ell\big\rangle$ (in units of U_o) and overlap integrals $\big\langle f_{nm}|u_\ell\big\rangle$, thus become

$$\big|f_{nm}(r,\phi)\big\rangle = \delta_{n,0}\delta_{m,0} + (1-\delta_{n,0}\delta_{m,0})\left[1-\frac{n^2}{\xi_{m,n}^2}\right]^{-1/2}\frac{J_n(\xi_{m,n}r)}{J_n(\xi_{m,n})}\mathrm{e}^{\mathrm{i}n\phi}, \tag{5.1a}$$

$$\lambda_{nm} = (1-\delta_{n,0}\delta_{m,0})\,\xi_{m,n}^2, \quad n,m=0,1,2,\ldots, \tag{5.1b}$$

$$\big|u_\ell\big\rangle = \varepsilon_\ell\frac{8}{k_\ell^2}\left[\frac{J_0(k_\ell r)}{J_0(k_\ell)}-1\right], \quad k_\ell=\sqrt{-\mathrm{i}\ell\omega_o/Sc}, \tag{5.1c}$$

$$\big\langle f_{nm}|u_\ell\big\rangle = -\varepsilon_\ell\delta_{n,0}\left[\delta_{\ell,0}\frac{8}{\xi_{1,m}^2}+(1-\delta_{\ell,0})\frac{16}{(\xi_{1,m}^2-k_\ell^2)k_\ell}\frac{J_1(k_\ell)}{J_0(k_\ell)}\right]. \tag{5.1d}$$

Here J_n is the nth-order Bessel function, $\xi_{n,m}$ is the mth root of the derivative $J_n'(\xi_{n,m})=0$ and ε_ℓ is the relative amplitude of the ℓth Fourier component of the velocity field. We compute the remaining overlap integrals $\big\langle f_{0m}\big|u_\ell\big|f_{0m}\big\rangle$ in D_{eff}^{point} numerically. Note that axisymmetry of the velocity field implies that only the $n=0$ term can be non-zero in $\big\langle f_{nm}|u_\ell\big\rangle$ and the azimuthal angle ϕ drops out.

For the infinite parallel-plate channel of height h in the xy plane and aligned with the x-axis, the height coordinate z is normalized by the half-height $a=h/2$ such that $-1\leqslant z\leqslant 1$. Using the same length scale, the width coordinate is restrained to the interval $-R<y<R$, where R is a cutoff introduced to regularize the transverse diffusion eigenmodes. For an initial point concentration placed at $\boldsymbol{r}_\perp^o=(0,z_0)$, our analysis is thus *a priori* restricted to times less than the diffusion time R^2a^2/D where no molecules have had time to reach the cutoff at $y=\pm R$. The pair-index eigenmodes $\big|f_{nm}\big\rangle$, flow field Fourier components $\big|u_\ell\big\rangle$ (in units of U_o), and overlap integrals $\big\langle f_{nm}|u_\ell\big\rangle$ thus become

$$\big|f_{nm}(y,z)\big\rangle = \frac{2}{\sqrt{(1+\delta_{n,0})(1+\delta_{m,0})}}\cos\left[n\frac{\pi}{2}\left(1+\frac{y}{R}\right)\right]\cos\left[m\frac{\pi}{2}(1+z)\right] \tag{5.2a}$$

$$\lambda_{nm} = \left(\frac{n\pi}{2R}\right)^2+\left(\frac{m\pi}{2}\right)^2, \quad n,m=0,1,2,\ldots \tag{5.2b}$$

$$\big|u_\ell\big\rangle = \varepsilon_\ell\frac{3}{{k_\ell}^2}\left[\frac{\cos(k_\ell z)}{\cos(k_\ell)}-1\right], \quad k_\ell=\sqrt{-\mathrm{i}\ell Wo}, \tag{5.2c}$$

$$\big\langle f_{nm}|u_\ell\big\rangle = \varepsilon_\ell\frac{6\sqrt{2}\big(1+(-1)^m\big)\,\delta_{n,0}}{\sqrt{1+\delta_{m,0}}}\frac{\dfrac{1}{k_\ell}\tan(k_\ell)-\delta_{m,0}}{4{k_\ell}^2-m^2\pi^2}. \tag{5.2d}$$

The remaining overlap integrals $\big\langle f_{0m}\big|u_\ell\big|f_{0n}\big\rangle$ are computed numerically, but for the steady flow we find

$$\big\langle f_{0n}\big|u_0\big|f_{0m}\big\rangle = \left[1-\frac{3}{\pi^2m^2}\right]\delta_{m,n}-(1-\delta_{m,n})\,\frac{12\big[1+(-1)^{n+m}\big](m^2+n^2)}{\pi^2(m^2-n^2)^2}. \tag{5.2e}$$

Note that the y-independence of the velocity field implies that only the $n=0$ term can be non-zero in $\big\langle f_{nm}|u_\ell\big\rangle$. The resulting expressions thus depend neither on the width coordinate y nor on the value of the transverse cutoff R, and consequently the results are valid for all times following the release.

https://doi.org/10.1017/jfm.2014.324 Published online by Cambridge University Press

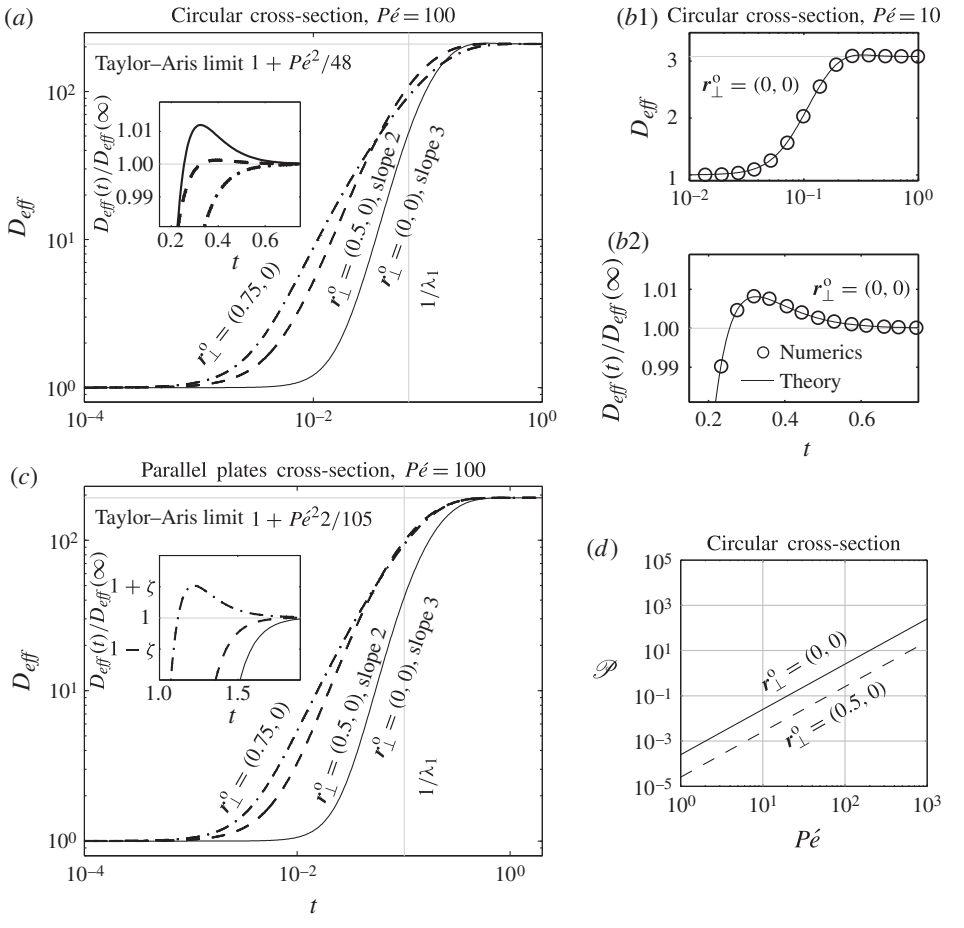


FIGURE 1. (*a*) Plot of $D_{eff}^{pnt,std}(t)$ of (3.6) in a circular cross-section at steady flow $Pé = 100$ with initial droplet position $\boldsymbol{r}_\perp^o = (r_0, \phi_0)$. It exhibits a peak with a relative amplitude of 1 % before relaxing to the Taylor–Aris limit (inset). (*b*1)–(*b*2) Comparison of the theory (line) for the circular cross-section with $\boldsymbol{r}_\perp^o = (0, 0)$ at $Pé = 10$ to axisymmetric direct numerical simulation (circles, see appendix A) of $D_{eff}^{pnt,std}(t)$ confirming the slope of the transient and the peak. (*c*) Plot of $D_{eff}^{pnt,std}(t)$ of (3.6) in a parallel-plate cross-section at steady flow $Pé = 100$ with $\boldsymbol{r}_\perp^o = (z_0, y_0)$. The relative peak amplitudes are markedly lower (less than $\zeta = 10^{-6}$, see inset) due to the lack of velocity gradients in the y direction. (*d*) Maximum peak amplitude $\mathscr{P} = \max_t\{\Delta D_{eff}^{pnt,std}(t)\}$ in a circular cross-section confirms the scaling $\mathscr{P} \propto Pé^2$ predicted by (6.2).

6. Point releases in steady flows

Using our analytical result for D_{eff}^{point}, we now study the transient development of the dispersion $D_{eff}^{pnt,std}(t)$ in steady flows. In figure 1(*a*,*b*) it is shown for times up to the Taylor–Aris limit for a circular cross-section with initial position $\boldsymbol{r}_\perp^o = (r_0, \phi_0)$ and in figure 1(*c*) for a parallel-plates channel with $\boldsymbol{r}_\perp^o = (z_0, y_0)$. Note that we have confirmed our analytical results by direct numerical simulation in figure 1(*b*) with details of the numerical simulations given in appendix A.

https://doi.org/10.1017/jfm.2014.324 Published online by Cambridge University Press

6.1. *Scaling with time in the transient phase*

The initial phase dominated by molecular diffusion ($D_{eff}^{pnt,std} \approx D \propto t^0$) is followed by a transient phase where $D_{eff}^{pnt,std} \propto t^s$ with the $\boldsymbol{r}_\perp^o$-dependent exponent $s = s(\boldsymbol{r}_\perp^o) \geqslant 2$. Finally, $D_{eff}^{pnt,std}$ reaches the Taylor–Aris limit of complete transverse mixing with the time-independent dispersion $D_{eff}^{pnt,std} \propto t^0$. For the circular channel, off-axis releases $\boldsymbol{r}_\perp^o = (r, \phi_0)$ lead to the scaling $D_{eff}^{pnt,std} \propto t^2$, while an on-axis release $\boldsymbol{r}_\perp^o = (0, 0)$ leads to the dispersion $D_{eff}^{pnt,std} \propto t^3$ due to the vanishing of the on-axis radial velocity gradient. This scaling behaviour is the same for the two geometries, while the limiting value $D_{eff}^{point}(\infty)$ and the transverse diffusive time scale $1/\lambda_1$ of course do depend on the specific geometry. The initial position also affects the waiting time before the axial dispersion increases past pure diffusion; it is longer for channel-centre releases than for off-centre releases. This is in agreement with both short-time studies ignoring the wall (Foister & van de Ven 1980; Rhines & Young 1983; Latini & Bernoff 2001) and a study that employed a stochastic differential equation approach to specifically these two geometries including the confining wall (Camassa *et al.* 2010).

We can rationalize these temporal scalings using a simple physical model capturing the essentials of the phenomenon. Consider a Poiseuille velocity profile $u(r) \propto 1 - r^2$ in a circular channel, and let a point concentration be released at the position r_0. For short times, the radial diffusion of the solute is well described by molecular diffusion with a spread $\Delta r(t) \propto \sqrt{t}$ around r_0. This radial diffusion implies different axial displacements $\Delta x_\pm = \int u\big[r_0 \pm \Delta r(t)\big]\,\mathrm{d}t$. For the Poiseuille profile we find $\Delta x_\pm \propto (1 - r_0^2)t - (1/2)t^2 \mp (4/3)r_0 t^{3/2}$. With the centre of mass of the solute being displaced axially as $\bar{x} \propto u(r_0)t$, the variance about this centre of mass will scale as

$$\mu_2(t) = \big\langle (x - \bar{x})^2 | c \big\rangle \propto \tfrac{1}{2}\left[(\Delta x_- - \bar{x})^2 + (\Delta x_+ - \bar{x})^2\right] = \tfrac{1}{4}t^4 + \tfrac{16}{9}r_0^2 t^3. \tag{6.1}$$

Hence, in general the short-time scaling is $D_{eff}^{pnt,std} \propto \mathrm{d}\mu_2/\mathrm{d}t \propto t^2$, except when the initial release point is at the channel centre $r_0 = 0$, in which case $D_{eff}^{pnt,std} \propto t^3$. These scalings agree with the observations from figure 1. Due to diffusion across streamlines separating regions of different flow speeds, the transient dispersion along the direction of the flow proportional to t^2 or t^3 is faster even than the 'ballistic' dispersion by pure advection (i.e. $D_{eff}^{pnt,std} \propto t$). Furthermore, the difference in initial waiting time is a result of the small velocity gradients present in the vicinity of the centre axis. A point concentration starting at the centre axis must diffuse greater distances than off-axis release points to experience a substantial speed change which leads to the increase in $D_{eff}^{pnt,std}$ above unity. Hence, while it is powered by transverse diffusion, the transient in $D_{eff}^{pnt,std}$ at small times is caused by the advective stretching of the solute, and $D_{eff}^{pnt,std}$ is consequently not expected to be diffusive.

We observe that $D_{eff}^{pnt,std}(t)$ for $\boldsymbol{r}_\perp^o = (0.75, 0)$ in both cross-sections (panels *a* and *c*) for small times changes from a t^2 to t scaling, seemingly violating the explanation just given. This is because the solute in this case quickly begins to interact with the wall, which limits the different speeds sampled by the transversely diffusing solute. This effect is not included in the simple model. As the channel wall is always felt, similar to the case of transverse uniform initial distribution (see § 4), the speed variations sampled by the solute is smaller than for a bulk release, and this changes the scaling to $D_{eff}^{pnt,std} \propto t$.

https://doi.org/10.1017/jfm.2014.324 Published online by Cambridge University Press

6.2. *Peaks in the effective diffusivity*

Contrary to the transverse uniform case, peaks in $D_{eff}^{pnt,std}(t)$ exceeding the Taylor–Aris limit $D_{eff}(\infty)$ are observed in both geometries before this limit is finally reached, see the insets in figure 1(*a*,*c*). The existence of this phenomenon has also been confirmed by direct numerical simulation for a centreline initial position in a circular cross-section at $Pé = 10$ in figure 1(*b*2).

6.2.1. *Mathematical analysis*

Since the peaks exceed the dispersion for transverse uniform distributions, we can study the peaks by subtracting from (3.6) the dispersion from a transverse uniform initial distribution $D_{eff}^{unif}(t) = 1 + Pé^2 \sum_{n=1}^{\infty} |\langle f_n|u_0\rangle|^2/\lambda_n \left(1 - \mathrm{e}^{-\lambda_n t}\right)$ (Vedel & Bruus 2012). We therefore investigate $\Delta D_{eff}^{pnt,std}(t) = D_{eff}^{pnt,std}(t) - D_{eff}^{unif}(t)$ and write this using (3.7) as

$$\begin{aligned}\Delta D_{eff}^{pnt,std}(t) \;=\; Pé^2 \Bigg\{ & \sum_{n=1}^{\infty} \langle u_0|f_n\rangle \Bigg[f_n(\boldsymbol{r}_\perp^o) \left(\langle f_n|u_0|f_n\rangle - \langle u_0|1\rangle \right) t\, \mathrm{e}^{-\lambda_n t} \\ & + f_n^2(\boldsymbol{r}_\perp^o) \langle u_0|f_n\rangle \frac{\mathrm{e}^{-2\lambda_n t} - \mathrm{e}^{-\lambda_n t}}{\lambda_n} \Bigg] \\ & + \sum_{n=1}^{\infty} \sum_{\substack{m=1 \\ m\neq n}}^{\infty} f_n(\boldsymbol{r}_\perp^o) \langle u_0|f_m\rangle \Bigg[\langle f_m|u_0|f_n\rangle \frac{\mathrm{e}^{-\lambda_n t} - \mathrm{e}^{-\lambda_m t}}{\lambda_m - \lambda_n} \\ & + f_m(\boldsymbol{r}_\perp^o) \langle u_0|f_n\rangle \frac{\mathrm{e}^{-(\lambda_m+\lambda_n)t} - \mathrm{e}^{-\lambda_m t}}{\lambda_n} \Bigg] \Bigg\}. \end{aligned} \tag{6.2}$$

In the long-time limit, $t \gg 1/\lambda_1$, the above equation is dominated by the terms proportional to $t\,\mathrm{e}^{-\lambda_n t}$, since all other terms depends on time via decaying exponentials. These dominating terms express the difference in relaxation times to the steady state between the time rate of change of the first and second moments. Furthermore, in this long-time limit, these dominating terms are themselves dominated by the longest-surviving $n = 1$ mode, so $\Delta D_{eff}^{pnt,std}(t) \approx Pé^2 \langle u_0|f_1\rangle f_1(\boldsymbol{r}_\perp^o) \left(\langle f_1|u_0|f_1\rangle - \langle u_0|1\rangle \right) t\,\mathrm{e}^{-\lambda_1 t}$ for $t \gg 1/\lambda_1$. For $t \to \infty$ the exponential ensures that $\Delta D_{eff}^{pnt,std}(t \to \infty) = 0$, i.e. the retrieval of the Taylor–Aris limit as discussed previously in § 3. It also follows directly from (6.2) that $\Delta D_{eff}^{pnt,std}(0) = 0$, so for any initial position for which $\Delta D_{eff}^{pnt,std}(t) > 0$ in the long-time limit $t \gg 1/\lambda_1$ a peak is present in $D_{eff}^{pnt,std}(t)$, as this then is converging towards $D_{eff}^{unif}(\infty)$ from above. This corresponds to those situations where the prefactor $\langle u_0|f_1\rangle f_1(\boldsymbol{r}_\perp^o) \left(\langle f_1|u_0|f_1\rangle - \langle u_0|1\rangle \right)$ is positive in the dominant $n = 1$ term. Since D_{eff}^{point} is proportional to the slope of the variance μ_2, $D_{eff}^{point} \propto \mathrm{d}\mu_2/\mathrm{d}t$, this change in the sign of the slope of D_{eff}^{point} from positive prior to the peak to negative following the peak signifies an inflection point in μ_2. Correspondingly, the peak, along with this inflection point, is absent wherever $\langle u_0|f_1\rangle f_1(\boldsymbol{r}_\perp^o) \left(\langle f_1|u_0|f_1\rangle - \langle u_0|1\rangle \right) < 0$.

Mathematically, the peaks occur when the time derivative of the second moment relaxes slower than the time derivative of the square of the first moment, i.e. situations where the solute still disperses unevenly although the centre of mass has equilibrated. Since this depends on the transient interplay of flow field and solute distribution, it in general depends on the initial release position $\boldsymbol{r}_\perp^o$ in a complicated manner.

https://doi.org/10.1017/jfm.2014.324 Published online by Cambridge University Press

For the circular cross-section where the f_1 is given by (5.1*a*), $\langle f_1|u_0\rangle = -8/\xi_{1,1}^2$, (5.1*d*) and $\langle f_1|u_0|f_1\rangle = 4/3$, the prefactor to $G(t)$ is positive for $f_1(\boldsymbol{r}_\perp^o) < 0$, i.e. for $r_0 < \xi_{0,1}/\xi_{1,1} = 0.63$. For the parallel plates cross-section (where the lowest eigenstate present is f_{02}), the prefactor is positive for $|z_0| > 1/2$ according to (5.2*a*) and (5.2*d*) using $\langle f_{02}|u_0|f_{02}\rangle = 1 - 3/(4\pi^2) > 0$. These results are confirmed from figure 1(*a*,*c*,*d*). Furthermore, (6.2) illustrates that the peak amplitude has the normal scaling $\Delta D_{eff}^{pnt,std} \propto Pé^2$ also found for the Taylor–Aris dispersion increase, see figure 1(*d*) where we plot the maximum peak amplitude $\mathscr{P} = \max_t \Delta D_{eff}^{pnt,std}(t)$ as a function of *Pé*. Mathematically, these peaks are absent for transverse uniform initial solute distributions because the first and second moments relax on the same time scale (Vedel & Bruus 2012).

6.2.2. *Physical explanation*

Such peaks would not be expected in a dissipative process such as diffusion, but as discussed above, the transient is dominated by advection. This observation is key to understanding the phenomenon. While the solute diffuses from the channel centre to the walls on the time scale $1/\lambda_1$, the concentration field of an initial point release is not transversely uniform at this time, but remains concentrated towards the initial release position $\boldsymbol{r}_\perp^o$. Thus, while at the time $1/\lambda_1$ the Taylor–Aris effect of axial dispersion sets in as the centre of mass relaxes to the channel mean speed, the transversely non-uniform concentration field implies that more solute will diffuse transversely outward from the release point $\boldsymbol{r}_\perp^o$ than in the opposite direction. Therefore, the amount of solute moving from higher to lower speeds does not equal the opposite process, which transiently results in an enhanced axial spreading exceeding the Taylor–Aris limit $D_{eff}(\infty)$. As the transverse distribution eventually becomes uniform at a given axial position after the solute has made first contact with the wall, $D_{eff}^{pnt,std}(t)$ approaches $D_{eff}(\infty)$. It follows from these arguments and the mathematical analysis that the largest peaks are expected to occur for values of $\boldsymbol{r}_\perp^o$ that imply the spreading of solute in the largest velocity gradients (most pronounced variation in relaxation times between the first and second moments). For the parallel plates, see figure 1(*b*), the largest effect is found when the solute is released close to one of the walls ($|z_0| > 1/2$), because then the solute must pass through the high-gradient regions at both walls before reaching the opposite wall. For the circular tube, the effect is only present when starting towards the centre since the solute then reaches the circumference with its large velocity gradients more evenly, and a large peak in $D_{eff}^{pnt,std}$ results, see figure 1(*a*). This peak value is even larger than that of the parallel-plate channel because the circular tube has velocity gradients in two spatial dimensions contrary to the one dimension of the parallel-plate channel. No peak is observed if the solute is released close to the wall ($r_0 > \xi_{0,1}/\xi_{1,1} = 0.63$) because the solute will sample a mix of large gradients along the wall and small gradients towards the centre during the transient.

6.2.3. *Increased peak amplitude in a suitably chosen velocity field*

From the above explanation it is clear that a velocity profile with a larger radial velocity gradient should lead to an increased peak amplitude. To investigate this further, we used the velocity profile of a Ostwald–de Waele power-law fluid of exponent q which has the rheological relationship $\tau = \kappa\,(\partial u/\partial x)^q$ between shear stress τ and shear rate $\partial u/\partial x$ (Ostwald 1929; Bruus 2008). We applied it only to

https://doi.org/10.1017/jfm.2014.324 Published online by Cambridge University Press

Exponent q	10^{-1}	10^{0}	10^{1}	10^{2}	10^{3}	10^{4}	10^{5}
$\mathscr{P}_{rel}$ (%)	9×10^{-8}	1.201	3.500	3.886	3.926	3.930	3.931

TABLE 1. Maximum relative peak amplitude $\mathscr{P}_{rel}$, see (6.4), for a Ostwald–de Waele power-law fluid with exponent q, see (6.3). For the circular tube the velocity profiles are nearly flat for $q \ll 1$, parabolic for $q = 1$, and nearly linear for $q \gg 1$.

centreline releases in pressure-driven flow in the circular tube since the peaks are more pronounced here. The velocity profile in this fluid is

$$u(r) = \frac{1+3q}{1+q}\left[1 - r^{1+1/q}\right], \tag{6.3}$$

using the average channel speed $U_o = qa^2\left[2^{1/q}(1+3q)\right]^{-1}\left[\Delta p/(\mathscr{L}\kappa)\right]^{1/q}$ as the velocity scale. The case of $q = 1$ corresponds to a Newtonian fluid with the paraboloid velocity profile, $q < 1$ yields shear-thinning fluids (such as blood) with more plug-like velocity profiles and $q > 1$ corresponds to shear-thickening fluids (such as corn starch solutions) with more conic velocity profiles; the radial velocity profile becomes linear as q tends to infinity, $\lim_{q\to\infty} u(r) = 3\,(1-r)$. Thus, by increasing q we achieved a velocity profile with greater speed variations across the tube radius. The increase of the maximum value of $D_{eff}^{pnt,std}$ from the Taylor–Aris limit is indeed found to increase with q to as much as 3.9 %, see table 1 where we give the maximum relative peak amplitude $\mathscr{P}_{rel}$,

$$\mathscr{P}_{rel} = \frac{\max\limits_{t}\left\{D_{eff}^{pnt,std}(t)\right\} - D_{eff}^{pnt,std}(\infty)}{D_{eff}^{pnt,std}(\infty)}. \tag{6.4}$$

6.2.4. *Why have the peaks not previously been observed?*

Spatially localized initial release of the solute produces interesting inflection points in the variance μ_2, which gives rise to the peaks in the instantaneous change in dispersion D_{eff}^{point}. To the best of the authors' knowledge, this is the first report of such inflection points and peaks, and as shown above, the effect is also confirmed from numerics. While the differential dispersion D_{eff}^{point} studied in this paper is proportional to the slope of the variance, Camassa *et al.* (2010) did not observe the peaks using the integrated dispersion measure $D_{eff}^{Camassa}(t) = 1/t\int_0^t D_{eff}^{point}(t')\,\mathrm{d}t'$. Thus, normalizing by time rather than using the slope of the variance can hide these features, in addition to providing a less clear image of the instantaneous changes in dispersion. Furthermore, Latini & Bernoff (2001) did not observe the effect because it depends on the channel walls which they did not take into account. Unfortunately, the few reported experimental investigations of the temporal evolution of Taylor–Aris dispersion (Codd *et al.* 1999; Bontoux *et al.* 2006) have not included point releases, so the existence of the peaks still awaits experimental verification.

In general, the cross-sectional averages underlying Aris' method of moments are not easily interpreted for asymmetric initial solute distributions; it is e.g. not clear that the centre-of-mass well describes the behaviour of the entire distribution during the transient. Using the physically transparent framework presented here allows for easier analysis of the underlying physics, as illustrated by the identification of the root cause of the peaks, and hence for fuller exploitation of the powerful method of moments for non-trivial distributions.

https://doi.org/10.1017/jfm.2014.324 Published online by Cambridge University Press

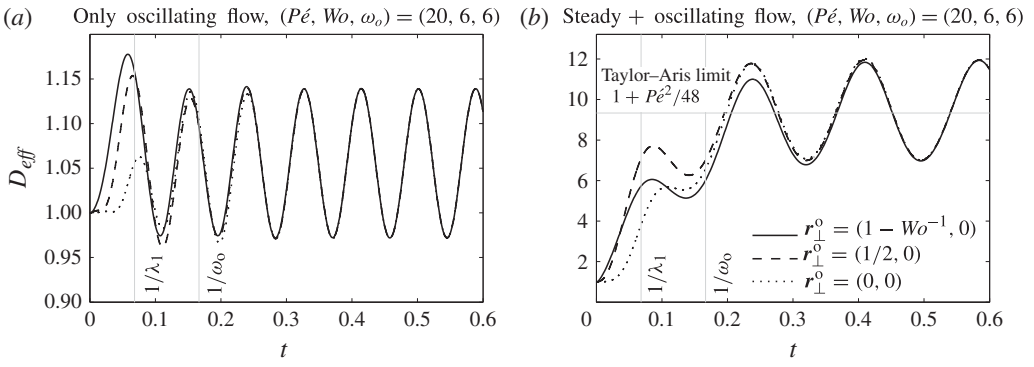


FIGURE 2. (*a*) The effective diffusivity $D_{eff}^{point}(t)$ in a purely oscillating (Womersley) flow at $(Pé, Wo, \omega_o) = (20, 6, 6)$ in the circular channel. Here D_{eff}^{point} exhibits a frequency-doubled response and its largest value is reached for the droplet released at the peak of the velocity boundary layer ($r_0 = 1 - Wo^{-1}$). (*b*) Plot of D_{eff}^{point} when adding a steady flow to the flow of (*a*). The largest value is now found by release points between the maximum of the steady flow component ($r = 0$) and the maximum of the oscillating flow component ($r = 1 - Wo^{-1}$). D_{eff}^{point} oscillates around the Taylor–Aris value $D_{eff}(\infty)$ for the purely steady flow. Legends are given in (*b*).

7. Unsteady flows

Our analytical expression (3.5) describes the exact behaviour of D_{eff}^{point} for any unsteady flow and any initial release position $\boldsymbol{r}_\perp^o$. The behaviour of D_{eff}^{point} for unsteady flows can in general be explained as a combination of the previous results for D_{eff} for transverse uniform initial concentrations in any time-dependent flow (Vedel & Bruus 2012), combined with the effects presented above which are particular to point releases in steady flows. Hence, a lengthy discussion of the evolution of D_{eff}^{point} is not warranted, and we will therefore only briefly touch on this subject here.

The velocity profile of a Newtonian fluid in a channel exposed to a harmonically varying pressure gradient changes systematically as the Womersley number *Wo*, the non-dimensional frequency of (3.4), is increased; this is in addition to its harmonic time dependence (Womersley 1955). At $Wo < 1$ the profile is the Poiseuille paraboloid, but as *Wo* increases past the first root of Bessel function J_0, the velocity profile will begin to deviate as shown in the inset of figure 2(*a*): since momentum can no longer diffuse across the entire channel to set up the Poiseuille profile, the maximum speed is at some times found in a boundary layer around the wall, implying that the fluid in the centre and within this boundary layer oscillate out of phase. The maximum value of the speed in this boundary layer is found at the diffusion distance from the wall set by the fluid oscillation frequency which in non-dimensional units is at the position $r = 1 - Wo^{-1}$ (Vedel, Olesen & Bruus 2010). Thus, releasing the point concentration here will produce the same effect as releasing it at the centre of the channel in steady Poiseuille flow; since this is the point where laterally diffusing solute will experience the greatest velocity gradients, the transient axial spreading is maximized at this release position. This is shown to be the case by the full line in figure 2(*a*) (computed for a circular tube), where furthermore the dashed and dotted lines are for a channel centre and intermediate release points, respectively. Furthermore, the phase lag between the velocity of the centre and the boundary layer of course means that

https://doi.org/10.1017/jfm.2014.324 Published online by Cambridge University Press

a similar phase lag will be found between two droplets released in the centre and within the boundary layer, respectively, as is also evident from figure 2(*a*).

The addition of a steady pressure gradient (of the same pressure amplitude) to the pulsating component yields an oscillating flow which is nonetheless always positive, and the position with the largest proximal speed variations is now no longer at $r = 1 - Wo^{-1}$ during the entire oscillation cycle; during the periods with a negative contribution from the oscillating flow component in the near-wall boundary layer, the channel centre speed will experience a positive contribution due to the transverse phase lag of the oscillating flow field. Hence, a position between the channel centre ($r = 0$) and the boundary layer ($r = 1 - Wo^{-1}$) will have the largest time-averaged proximal speed variations over a cycle, and will consequently experience the most significant transient axial spreading. This can be seen in figure 2(*b*) for the position $\boldsymbol{r}_\perp^o = (1/2,\ 0)$ which is clearly dominating during the transient. In general, the release position of the largest cycle-averaged proximal speed variations will have the most significant transient effects, even when more velocity frequencies are added. Naturally, this position shifts as more frequencies are added. Nonetheless, our formula (3.5) captures and contains all of these effects, and can be used to determine exactly where this 'optimal' position is for any given flow, channel cross-section and release position $\boldsymbol{r}_\perp^o$.

8. Conclusion and outlook

Using our previously described framework (Vedel & Bruus 2012), we have in this paper presented a general expression for the dispersion $D_{eff}^{point}(t)$ of initial point concentrations in steady and unsteady flows in a long straight channel having any constant cross-section. While our formal expressions in §§ 3 and 4 have not been investigated for convergence properties, we have found excellent agreement between specific theoretical predictions obtained from these general expressions and numerical simulations in both § 6 as well as our previous paper (Vedel & Bruus 2012). Focusing on the transient phase prior to the well-described Taylor–Aris limit, we have showed that transient anomalous diffusion with release-point-dependent temporal scaling is a hallmark of Taylor–Aris dispersion for any channel cross-section, and have furthermore identified and analysed peaks in D_{eff}^{point} exceeding the Taylor–Aris limit arising from inflection points in the solute variance μ_2. In addition, we have showed and explained how the aforementioned effects are modulated in a time-dependent flow. All of these effects can be understood as consequences of the involved fundamental processes of solute diffusion, fluid momentum diffusion and local velocity gradients. Moreover, our work has illustrated that the cross-sectional averages used in Taylor–Aris dispersion theory are not representative of an initial point concentration before it fills a substantial part of the channel (in the transverse direction), so the transient advective stretching of the point concentration is convoluted with the rest of the channel to produce what appears at a glance as physically counterintuitive results. Using the framework presented in this paper provides a deeper insight into the structure of the solution and thereby extends the possibilities of Aris' method of moments without abandoning physical understanding.

In addition to its scientific relevance, the predicted transients in D_{eff}^{point} persist long enough in physical systems that it has important implications for medical and industrial applications. Since it decays on a non-dimensional time scale of $1/\lambda_1$, which is typically of the order of 10^{-1} (Vedel & Bruus 2012), and since the normalization time scale is given by diffusion as L_o^2/D, decay of the transient for a solute with

https://doi.org/10.1017/jfm.2014.324 Published online by Cambridge University Press

$D = 10^{-10}$ m^2 s^{-1} in 1000 s will only occur in channels with $L_o \leqslant 10^{-3}$ m; these time scales are long compared to the resting times for drug delivery and many industrial applications, so the non-symmetric solute distributions and rapid spreading associated with the transient are present long enough that they cannot be ignored. In unsteady flows such transiently asymmetric solute distributions coupled with our previous finding that the dispersion under certain conditions in such flows can reach a steady state exceeding the normal Taylor–Aris limit suggests that radially uneven absorption of e.g. injected drugs could occur over unexpectedly long distances of the arteries. Furthermore, recent findings of Taylor–Aris dispersion for solutes acting as signals and nutrition within biofilms (Davit *et al.* 2013) suggests that our results may also be useful in the growing community of biofilm control, for which both the promotion of desirable biofilms (for e.g. wastewater treatment) as well as the inhibition of undesirable biofilms (e.g. microbially influenced corrosion in pipelines, chronic infections) are major goals.

Acknowledgements

We wish to thank our referees for insightful comments and remarks which have helped us significantly to improve the paper. In particular, one referee pointed out the lack of mathematical analysis concerning the existence of the peaks discussed in § 6.2, and provided a first proof in the special case of parallel plates. Based on this proof we developed the general proof given in § 6.2.1. This research was supported by grant no. 2106-08-0018 'ProCell', under the Programme Commission on Strategic Growth Technologies, the Danish Agency for Science, Technology and Innovation.

Appendix A. Numerics

A.1. *Direct numerical simulations*

Using the commercial finite-element package COMSOL MULTIPHYSICS version 3.5a, we have calculated $D_{eff}(t)$ numerically directly from the definition (3.1) by solving for the concentration field c in the governing advection–diffusion equation using the analytical solutions for the velocity field as input. From the obtained $c(\boldsymbol{r}, t)$ field we determined $M_1(t)$, $\mathrm{d}M_1(t)/\mathrm{d}t$ and $\mathrm{d}M_2(t)/\mathrm{d}t$, and from these $D_{eff}(t)$. The azimuthal symmetry was exploited for computational efficiency and the solution was furthermore computed in a frame of reference traveling with the mean speed of the flow. We used a Gaussian initial distribution placed at $(r, z) = (0, 0)$ with variance corresponding to an elapsed time of $t = 10^{-4}$ since release (non-dimensional units), which is much lower than $t \approx 10^{-2}$ where the distribution begins to deviate from the Gaussian, see figure 1.

To ensure mass conservation, the number of mesh elements was chosen so that the local Péclet number in each cell (as given by the velocity in the mesh element, the mesh element length and the molecular diffusivity) did not exceed 0.5, which corresponds to the requirement that the maximal mesh element length is $L_{mesh} = (2\,Pé)^{-1}$. Furthermore, we increased the mesh resolution in a small box of non-dimensional length 0.2 around the solute release position to ensure good resolution of the short-time dynamics, using a resolution in this domain of $L_{mesh}/50$. Interpolation between the two meshing length scales were achieved by requiring a maximum relative mesh element growth rate of 1.1. The high mesh resolution locally around the release point combined with the mass-conservation considerations limited the solution to $Pé \lesssim 12$ on a dedicated 12 core, 48 GB RAM computer, where each solution took $\sim$24 h to complete. Owing to these severe limitations, off-centreline

https://doi.org/10.1017/jfm.2014.324 Published online by Cambridge University Press

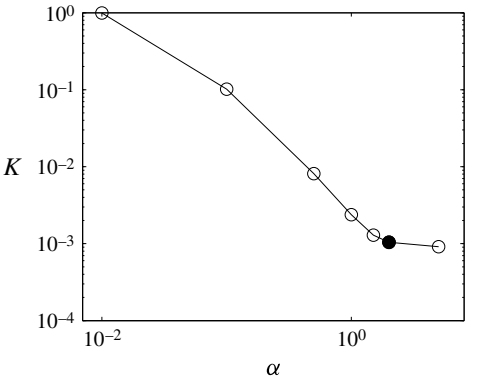


FIGURE 3. Mesh-convergence plot of the figure of merit K from (A 1) versus the mesh element parameter α, where the smaller values of the latter correspond to larger mesh elements. Convergence is achieved around $\alpha = 2$ (filled circle) and we consequently used this value for the simulations in figure 1(*b*).

initial positions in the circular cross-section and simulations in the parallel-plate cross-section were not investigated.

In order to verify the correctness of our numerical solutions, we present in figure 3 a mesh-convergence analysis by comparing the solutions for decreasing sizes of $L_{mesh} = 1/(\alpha\, Pé)$ (increasing values of α) using the convergence measure

$$K(\alpha) = \sqrt{\frac{\sum_i \left[D_{eff}^{num}(\alpha; t_i) - D_{eff}(t_i)\right]^2}{\sum_i D_{eff}(t_i)^2}}, \tag{A 1}$$

where $D_{eff}^{num}(\alpha; t)$ is the numerically computed effective diffusivity for a given value of the mesh-resolution parameter α while $D_{eff}(t)$ is the effective diffusivity of (3.6). We use the parameter α to obtain a mesh parametrization which is independent of the Péclet number, since in general the mesh element size must scale with the inverse of $Pé$ to achieve mass conservation (cell Péclet numbers below unity). Figure 3 (computed at $Pé = 3$) shows that convergence has been obtained for the used value of $\alpha = 2$ indicated by the filled circle.

A.2. *Evaluation of our theoretical formulae*

Numerical evaluations of our theoretical expressions for (3.5) and (3.6) were obtained by truncating the sums after 100 terms; the inclusion of additional terms did not further improve the results. Additional numerical tricks for speeding up the evaluation of these sums were described in our previous paper (Vedel & Bruus 2012).

REFERENCES

AJDARI, A., BONTOUX, N. & STONE, H. A. 2006 Hydrodynamic dispersion in shallow microchannels: the effect of cross-sectional shape. *Anal. Chem.* **78**, 387–392.

https://doi.org/10.1017/jfm.2014.324 Published online by Cambridge University Press

ARIS, R. 1956 On the dispersion of a solute in a fluid flowing through a tube. *Proc. R. Soc. Lond.* A **235** (1200), 67–77.

ARIS, R. 1960 On the dispersion of solute in pulsating flow through a tube. *Proc. R. Soc. Lond.* A **259** (1298), 370–376.

BARTON, N. G. 1983 On the method of moments for solute dispersion. *J. Fluid Mech.* **126**, 205–218.

BONTOUX, N., PÉPIN, A., CHEN, Y., AJDARI, A. & STONE, H. A. 2006 Experimental characterization of hydrodynamic dispersion in shallow microchannels. *Lab Chip* **6**, 930–935.

BRUUS, H. 2008 *Theoretical Microfluidics*. Oxford University Press.

CAMASSA, R., LIN, Z. & MCLAUGHLIN, R. 2010 The exact evolution of scalar variance in pipe and channel flow. *Commun. Math. Sci.* **8** (2), 601–626.

CODD, S. L., MANZ, B., SEYMOUR, J. D. & CALLAGHAN, P. T. 1999 Taylor dispersion and molecular displacements in Poiseuille flow. *Phys. Rev.* E **60**, R3491–R3494.

DAVIT, Y., BYRNE, H., OSBORNE, J., PITT-FRANCIS, J., GAVAGHAN, D. & QUINTARD, M. 2013 Hydrodynamic dispersion within porous biofilms. *Phys. Rev.* E **87**, 012718.

FALLON, M. S., HOWELL, B. A. & CHAUHAN, A. 2009 Importance of Taylor dispersion in pharmacokinetic and multiple indicator dilution modeling. *Math. Med. Biol.* **26**, 263–296.

FOISTER, R. T. & VAN DE VEN, T. G. M. 1980 Diffusion of Brownian particles in shear flows. *J. Fluid Mech.* **96**, 105–132.

LATINI, M. & BERNOFF, A. J. 2001 Transient anomalous diffusion in Poiseuille flow. *J. Fluid Mech.* **441**, 399–411.

LEIGHTON, D. T. 1989 Diffusion from an intial point distribution in an unbounded oscillating simple shear flow. *Physico-Chem. Hydrodyn.* **11**, 377–386.

MEHTA, M. L. 2004 *Random Matrices*, 3rd edn. Pure and Applied Mathematics, vol. 142. Elsevier/Academic Press.

MUKHERJEE, A. & MAZUMDER, B. S. 1988 Dispersion of contaminant in oscillatory flows. *Acta Mech.* **74**, 107.

OSTWALD, W. 1929 On the arithmetical representation of viscosity structural fields. *Kolloidn. Z.* **47** (2), 176–187.

PAUL, S. & MAZUMDER, B. S. 2008 Dispersion in unsteady Couette–Poiseuille flows. *Intl J. Engng Sci.* **46**, 1203–1217.

RHINES, P. B. & YOUNG, W. R. 1983 How rapidly is a passive scalar mixed within closed streamlines?. *J. Fluid Mech.* **133**, 133–145.

TAYLOR, G. I. 1953 Dispersion of soluble matter in solvent flowing slowly through a tube. *Proc. R. Soc. Lond.* A **219** (1137), 186.

VEDEL, S. & BRUUS, H. 2012 Transient Taylor–Aris dispersion for time-dependent flows in straight channels. *J. Fluid Mech.* **691**, 95–122.

VEDEL, S., OLESEN, L. H. & BRUUS, H. 2010 Pulsatile microfluidics as an analytical tool for determining the dynamic characteristics of microfluidic systems. *J. Micromech. Microengng* **20**, 035026.

WATSON, E. J. 1983 Diffusion in oscillatory pipe flow. *J. Fluid Mech.* **133**, 233–244.

WOMERSLEY, J. R. 1955 Method for the calculation of velocity, rate of flow and viscous drag in arteries when the pressure gradient is known. *J. Physiol.* **127**, 553–563.

https://doi.org/10.1017/jfm.2014.324 Published online by Cambridge University Press